Journal of Southeast University (English Edition) Vol. 37, No. 2, pp. 119 - 127 June 2021 ISSN 1003—7985

Effects of crankpin bearing speed and dimension on engine power

Nguyen Van Liem[1,2,3] Zhang Jianrun[1] Jiao Renqiang[2] Huang Dacheng[1]

([1]School of Mechanical Engineering, Southeast University, Nanjing 211189, China)

([2]School of Mechanical and Electrical Engineering, Hubei Polytechnic University, Huangshi 435003, China)

([3]Faculty of Automotive and Power Machinery Engineering, Thai Nguyen University of Technology, Thai Nguyen 23000, Vietnam)

Abstract: A new method combining the slider-crank mechanism dynamic (SCM) and crankpin bearing (CB) lubrication models is proposed to analyze the effects of CB dimensions and engine speed on the lubrication efficiency and friction power loss (LE-FPL) of an engine. The dynamic and lubrication equations are then solved on the basis of the combined model via an algorithm developed in MATLAB. To enhance the reliability of the research results, the experimental data of combustion gas pressure is applied for simulation. The load bearing capacity (or oil film pressure), friction force, friction coefficient, and eccentricity ratio of the CB are selected as objective functions to evaluate the LE-FPL. The effects of engine speed, bearing width, and bearing radius on the LE-FPL are then evaluated. Results show that reductions in engine speed, bearing width, or bearing radius can decrease the FPL but reduce the LE of the engine and vice versa. In particular, the LE-FPL can effectively be improved by slightly reducing the bearing width and bearing radius or maintaining engine speed at 2 000 r/min.

Key words: slider-crank mechanism; crankpin bearing; lubrication performance; friction loss

DOI: 10.3969/j.issn.1003-7985.2021.02.001

Given greater demands for fuel economy, energy conservation, and emission reduction in oil-fueled automobiles, technologies that can reduce friction power losses (FPLs) to improve the power of internal combustion engines (ICE) is a major concern for designers. The main causes of engine power loss include the friction between the piston skirt and the ring against the cylinder bore during motion and the friction between moving surface pairs of joints in the slider-crank mechanism (SCM) [1-3].

Studies on the influence of various SCM design parameters, the inertial mass of the piston, and the eccentricity between the crankshaft and cylinder centers on the horizontal impact force of the piston in the cylinder bore have been carried out over the last few decades[4-6]. Friction and noise vibration between the piston skirt and ring around the cylinder bore could significantly be reduced by optimizing the structure of the SCM. Optimization studies have also investigated the characteristics of lubrication factors, such as the friction force F and friction coefficient μ, between the moving surfaces of a piston and cylinder[1-2,6-7]. Researchers have found that FPLs are significantly reduced when a stable oil film exists on the lubricating surfaces.

The lubrication model of crankpin bearings (CBs) under an external load acting on the shaft moving at high speed was previously studied to illustrate the stability of the lubricating oil film thickness h on the friction surface pairs of the engine[8-10] according to the evaluation indices of load bearing capacity (LBC) and F. Results showed that the stability of h greatly depends on the pressure generated by the oil film. The effects of several factors, such as the temperature[11], radial clearance[7, 12-13], and load and speed of the shaft, on the oil film pressure have also been discussed[9-11, 14]. Previous studies mainly assessed the lubrication efficiency (LE) of the CB under the condition of a static load on a shaft moving at high speed. In actual applications, the shear stress of the oil film generated under various speeds and the dimensions of the CB could affect the resistance of the oil film. Moreover, in the working cycle of an ICE, the dynamic load acting on the CB changes very quickly under various engine speeds ω in terms of direction and intensity. Therefore, the effects of ω and CB dimensions should be taken into account during analyses of the LE-FPL of an engine. However, investigations on the LE-FPL of engines considering ω and CB dimensions together have rarely been reported.

The current study establishes a new numerical method by coupling the SCM dynamic and CB lubrication models to investigate their effect on the LE-FPL of an engine. An algorithm program based on the hybrid model was developed in MATLAB, and numerical simulations were performed to solve the hydrodynamic equations of the SCM

Received 2020-07-14, **Revised** 2021-04-20.

Biographies: Nguyen Van Liem (1986—), male, doctor; Zhang Jianrun (corresponding author), male, doctor, professor, zhangjr@seu.edu.cn.

Foundation items: The National Key Research and Development Plan (No. 2019YFB2006402), the Key Project of Scientific Research Plan of Hubei Polytechnic University (No. 21xjz02A), the Open Fund Project of Hubei Key Laboratory of Intelligent Transportation Technology and Device, Hubei Polytechnic University (No. 2020XY105, 2020XZ107).

Citation: Nguyen Van Liem, Zhang Jianrun, Jiao Renqiang, et al. Effects of crankpin bearing speed and dimension on engine power[J]. Journal of Southeast University (English Edition), 2021, 37(2): 119 - 127. DOI: 10.3969/j.issn.1003-7985.2021.02.001.

and CB. The LBC, F, μ, and eccentricity ratio ε between the shaft and bearing were then selected as objective functions. Finally, the influence of ω, bearing radius r_b, and bearing width B on the LE-FPL was clarified.

1 SCM Dynamic and CB Lubrication Models

1.1 SCM dynamic model

Assuming that the center of a crankshaft coincides with the cylinder center, the SCM dynamic model can be established as shown in Fig. 1. Here, L and R are the connecting rod length and rotation radius of the crankshaft, respectively; P is the combustion gas pressure acting on the piston peak; N and F_c are the piston forces impacting on the cylinder wall and connecting rod, respectively; F is the total force of the piston; F_{ic}, F_{c1}, and F_{c2} are the respective centrifugal inertial, radial, and tangent forces of the large-rod-end mass of the connecting rod impacting on the CB; F_{ip} is the inertial force of the small-rod-end and piston; W_0 is the impacting force on the CB; and φ and ω are the respective angle and angular velocity of the crankshaft.

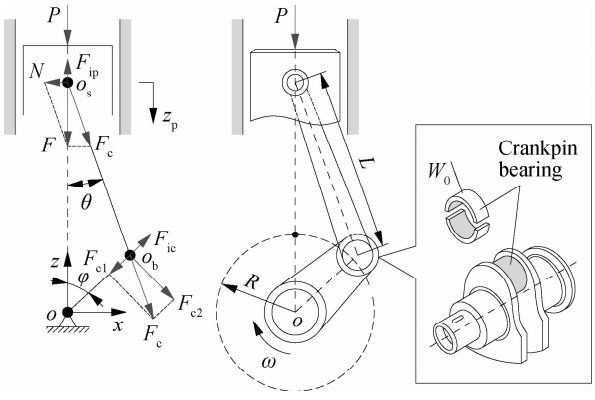

(a) (b)

Fig. 1 SCM model and its lubrication joints. (a) SCM dynamic system; (b) Lubrication joints

The piston's motion can be determined as

$$z_p = L + R - R\cos\varphi - L\cos\theta \tag{1}$$

The kinematic relation of SCM can be determined by

$$\left.\begin{aligned} R\sin\varphi &= L\sin\theta \\ \cos\theta &= 1 - 0.5\lambda^2\sin^2\varphi \end{aligned}\right\} \tag{2}$$

where $\lambda = R/L$ is the ratio between the rotation radius of the crankshaft and the length of the connecting rod.

Substituting Eq. (2) into Eq. (1), the piston's motion and acceleration can be rewritten as

$$z_p = R\left(1 - \cos\varphi + \frac{\lambda}{4(1 - \cos 2\varphi)}\right) \tag{3}$$

$$\ddot{z}_p = R\omega^2(\cos\varphi + \lambda\cos 2\varphi) \tag{4}$$

where $\omega = \dot{\varphi} = \mathrm{d}\varphi/\mathrm{d}t$.

m_{sc} and m_{bc} are assumed to be the lumped masses of the small- and large-rod-ends of the connecting rod at o_s and o_b, respectively. Thus, the F_{ip} of the small-rod-end and piston is written as

$$F_{ip} = -(m_{sc} + m_p)R\omega^2(\cos\varphi + \lambda\cos 2\varphi) \tag{5}$$

where m_p is the piston mass.

Under the impact of P on the piston peak, the dynamic forces impacting the cylinder wall and connecting rod can be determined by

$$\left.\begin{aligned} N &= F\tan\theta = (F_{ip} + P)\tan\theta \\ F_c &= \frac{F}{\cos\theta} = \frac{F_{ip} + P}{\cos\theta} \end{aligned}\right\} \tag{6}$$

The impact of F_c, which has two components of tangential and radial forces, on the CB is determined by

$$\left.\begin{aligned} F_{c1} &= F_c\cos(\theta + \varphi) \\ F_{c2} &= F_c\sin(\theta + \varphi) \end{aligned}\right\} \tag{7}$$

The large-rod-end mass of the connecting rod is rotated with ω, and its F_{ic} can be defined as

$$F_{ic} = -m_{bc}R\omega^2 \tag{8}$$

The bearing of the connecting rod provides a rotating motion and transmits loads between the large-rod-end and crankpin. Thus, the dynamic load W_0 of the connecting rod impacting on the CB is determined by

$$W_0 = \sqrt{(F_{c1} + F_{ic})^2 + F_{c2}^2} \tag{9}$$

Changes in W_0 in both direction and intensity could be applied to analyze the LE-FPL of the CB.

1.2 CB lubrication model

1.2.1 Lubrication model in the computational region

In the working cycle of the engine, the crankpin is impacted by W_0 and rotated with an angular velocity ω inside the bearing of the connecting rod, as shown in Fig. 1. Therefore, the LE-FPL of the CB could be evaluated by modeling the crankpin under the impact of W_0 and rotated at ω inside the bearing as shown in Fig. 2.

In Fig. 2, B and r_b are the bearing width and radius, respectively; r_s is the shaft radius and $r_s < r_b$; e and $\varepsilon = e/c$ $(0 < \varepsilon < 1)$ are the eccentricity and eccentricity ratio between the center of the bearing and shaft, respectively; $c = r_b - r_s$ is the radial clearance between the shaft and bearing fully filled with the lubricant to create the hydrodynamic pressure p; $u_0 = \omega r_b$ is the relative velocity between the CB surfaces; and ψ is the attitude angle. Then, h can be determined from the CB lubrication model as

$$h = r_b - r_s + e\cos\varphi = c(1 + \varepsilon\cos\varphi) \tag{10}$$

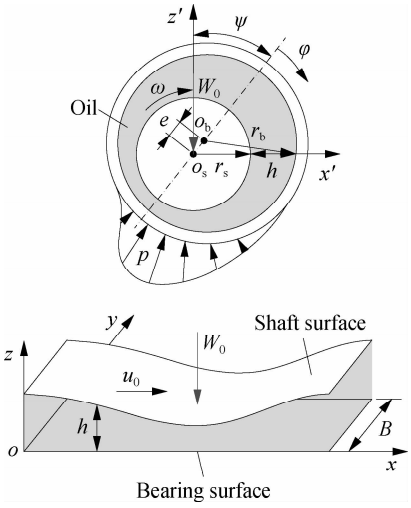

Fig. 2 The CB hydrodynamic model

1.2.2 Application of the Reynolds equations

Assume that the bearing surface is fixed in the x- and y-directions and that the shaft surface only moves with a constant velocity u_0 in the x-direction, as seen in Fig. 2. The boundary conditions of the fluid velocity on the CB surface in the x- and y-directions are determined by

$$\left.\begin{aligned} u\mid_{z=h} &= u_0 \quad \text{with shaft surface} \\ u\mid_{z=0} &= 0 \quad \text{with bearing surface} \end{aligned}\right\} \tag{11}$$

The lubricant density and viscosity are also assumed to be constant, and the influence of the inertia of the lubricant flow on the working process is negligible. Therefore, the pressure distribution of the lubrication film can be described as [11, 15]

$$\left.\begin{aligned} \frac{\partial p}{\partial x} &= \frac{\partial \tau}{\partial z} = \frac{\partial}{\partial z}\left(\eta \frac{\partial u}{\partial z}\right) \\ \frac{\partial p}{\partial y} &= \frac{\partial \tau}{\partial z} = \frac{\partial}{\partial z}\left(\eta \frac{\partial v}{\partial z}\right) \end{aligned}\right\} \tag{12}$$

Taking the second integral of Eq. (12) with respect to z and considering the initial conditions in Eq. (11), the velocity fluid equations are written as

$$\left.\begin{aligned} u &= \frac{1}{2\eta}\frac{\partial p}{\partial x}(z^2 - hz) + u_0 \frac{z}{h} \\ v &= \frac{1}{2\eta}\frac{\partial p}{\partial y}(z^2 - hz) \end{aligned}\right\} \tag{13}$$

where η is the dynamic viscosity of the oil film.

The volumetric flows of q_x and q_y in the x- and y-directions are calculated by integrating Eq. (13) over the z-direction and written as

$$\left.\begin{aligned} q_x &= \int_0^h u\mathrm{d}z = -\frac{h^3}{12\eta}\frac{\partial p}{\partial x} + u_0 \frac{h}{2} \\ q_y &= \int_0^h v\mathrm{d}z = -\frac{h^3}{12\eta}\frac{\partial p}{\partial y} \end{aligned}\right\} \tag{14}$$

The equation of the fluid continuity condition is given by

$$\left[\frac{\partial(\rho u)}{\partial x} + \frac{\partial(\rho v)}{\partial y} + \frac{\partial(\rho \tilde{\omega})}{\partial z}\right] + \frac{\partial \rho}{\partial t} = 0 \tag{15}$$

where ρ is the fluid density; u and v are the fluid velocities in the x- and y-directions, respectively, as determined in Eq. (13); and $\tilde{\omega}$ is the fluid velocity in the z-direction.

Because $\tilde{\omega}$ in the z-direction is very small, we can assume that $\tilde{\omega} = 0$ and ρ is a constant. Thus, the integral of Eq. (14) in the z-direction is

$$\frac{\partial}{\partial x}\left(\int_0^h u\mathrm{d}z\right) + \frac{\partial}{\partial y}\left(\int_0^h v\mathrm{d}z\right) + \frac{\partial}{\partial t}\left(\int_0^h \mathrm{d}z\right) = 0 \tag{16}$$

In Eq. (10), the oil film thickness h is constantly changing according to the rotation angle φ. Thus, the substitution of Eq. (14) into (16) and mathematical transformation lead to a new form of Eq. (16) [16-17],

$$\frac{\partial}{\partial x}\left(h^3 \frac{\partial p}{\partial x}\right) + \frac{\partial}{\partial y}\left(h^3 \frac{\partial p}{\partial y}\right) = 6\eta u_0 \frac{\partial h}{\partial x} + 12\eta \frac{\partial h}{\partial t} \tag{17}$$

The dimensionless form of the Reynolds equation in Eq. (17) can be expressed as

$$\beta^2 \frac{\partial}{\partial \varphi}\left(H^3 \frac{\partial P}{\partial \varphi}\right) + \frac{\partial}{\partial Y}\left(H^3 \frac{\partial P}{\partial Y}\right) = \Pi \frac{\partial H}{\partial \varphi} + \Lambda \frac{\partial H}{\partial T} \tag{18}$$

where $\beta = B/r_b$, $H = h/c$, $\varphi = x/r_b$, $Y = y/B$, $P = p/p_0$, $T = t/t_0$, $\Pi = 6\eta\omega B^2/(c^2 p_0)$, $\Lambda = 12\eta B^2/(c^2 p_0 t_0)$, and $p_0 = 101.325$ kPa.

The boundary conditions must be determined to obtain the pressure distribution of the oil film over the computational domain of Eq. (17). In this study, we assume that h exists over the CB surfaces and that the inlet and outlet lubricants are at the maximum position of h. The ambient pressure around the CB and the inlet and outlet pressures are equal to the atmospheric pressure p_0. The computational region Γ of the CB is plotted in Fig. 3. Here, i and f are the respective boundary lines of the initial and final pressures at the maximum position of h corresponding to $\varphi = 0°$ and 360°, and r and l are the respective boundary lines of the right and left pressures of the bearing at $y = 0$ and B.

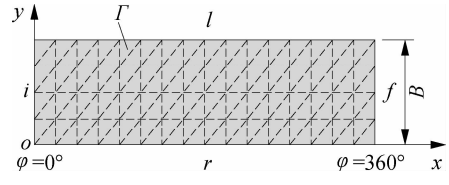

Fig. 3 CB computational region and meshing diagram

The boundary conditions of the oil film pressure can be written as

$$\left.\begin{aligned} p\mid_{\varphi=0°} &= p\mid_{\varphi=360°} \\ p\mid_{y=0} &= p\mid_{y=B} = 0 \end{aligned}\right\} \tag{19}$$

In general, the oil film in the small gap of the CB can usually be divided into the liquid and cavitation zones when the oil film is ruptured[11]. Because negative pressure due to gas dissolution and cavitation effects exists, Eq. (17) above cannot be used to calculate the cavitation region [18–19]. Thus, instead of ignoring negative pressures in the cavitation zone, only pressures below the saturation pressure p_s are varied to achieve the effective pressure p_e[15]. The oil film pressure in the cavitation zone can then be expressed as

$$p_e = \begin{cases} p_s & \text{if } p < p_s \\ p & \text{else} \end{cases} \tag{20}$$

1.2.3 Lubrication forces of mixed hydrodynamics

Under the impact of W_0 on the CB, the LBC of the oil film pressure generated in Γ can be determined by [16]

$$W = \sqrt{\left(-\iint_\Gamma p_e \cos\varphi \mathrm{d}x\mathrm{d}y\right)^2 + \left(-\iint_\Gamma p_e \sin\varphi \mathrm{d}x\mathrm{d}y\right)^2} \tag{21}$$

where load bearing capacity W equals the dynamic load W_0 on the CB.

F generated from the interfacial shear stress τ acting on the shaft in Γ can be calculated by[17]

$$\mathrm{F} = \iint_\Gamma \tau \mathrm{d}x\mathrm{d}y = \iint_\Gamma \left(\frac{h}{2}\frac{\partial p_e}{\partial x} + u_0\frac{\eta}{h}\right)\mathrm{d}x\mathrm{d}y \tag{22}$$

When W and F are obtained, the μ of the CB can be given by [15]

$$\mu = \frac{F}{W} \tag{23}$$

In this study, the W, F, μ, and ε between the shaft and bearing are selected as indices to evaluate the LE-FPL of the engine.

2 Algorithm

An algorithm written in MATLAB was used to estimate the objective functions and solve the equations of the system models. The simulation process includes three main steps as follows.

Step 1 The initial parameters that must be set include the dimensions of the SCM and CB, the combustion pressure on the piston peak, the zero matrices of the oil film pressure and shear stress ($a \times b$), and the zero matrices of the force vectors ($1 \times b$). The W_0 and coefficients of Eq. (18) are then calculated, and the initial pressure and shear stress matrices are also determined. Herein, the number of grid nodes is $a = b = 120$.

Step 2 When the pressure and shear stress have been determined, the initial LE-FPL can be obtained. In theory, W equals W_0. However, in actual conditions, W is not in equilibrium with W_0; thus, the computational algorithm cannot give the stopping condition for the computational process. This issue is addressed by setting a stopping condition of $W_0 - W_0 \leqslant \zeta$ with a very small value of ζ. Reaching the stop condition means that the difference between W_b and W_0 is very small. In this case, the distribution of the oil film pressure and shear stress in Γ and ε between the journal and bearing are considered acceptable, and the computational algorithm is stopped. The computational algorithm is continuously performed until the stopping condition is satisfied.

Step 3 The time required to complete a cycle of the engine corresponding to a crankshaft rotation angle of 720° is t_0. Parameter t_0 is divided into 120 equal parts, and t refers to each time node corresponding to a crankshaft rotational angle of $t' = 6°$. The oil film pressure and shear stress are calculated at each time t, and the computational algorithm is continued for the next loop at $t = t + t'$ until $t \geqslant t_0$. The complete computational algorithm and objective functions of the LE-FPL are finally obtained. A schematic of the calculation process is provided in Fig. 4.

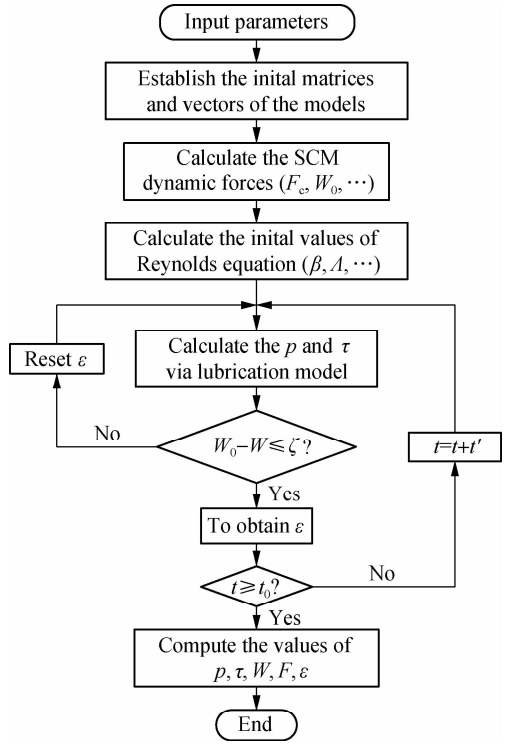

Fig. 4 Flowchart of the algorithm of the computational model

3 Simulation Results and Analysis

The necessary parameters for simulation listed in Tab. 1 and the combustion gas pressure acting on the piston peak, which is obtained from the experimental data in Ref. [14], as shown in Fig. 5(a), were applied to calculate W_0 under various ω and analyze the LE-FPL. The W_0 results are plotted in Fig. 5(b).

As shown in Fig. 5(b), the impact load is constantly varied under different ω and rotation angles. As the

Tab. 1 Parameters of the SCM and CB

Parameters	Values	Parameters	Values
m_p/kg	0.264	B/mm	20
m_{bc}/kg	0.345	r_b/mm	25
m_{sr}/kg	0.095	p_0/kPa	101.325
m_{br}/kg	0.250	φ/(°)	0-720
L/mm	129.5	c/μm	10
R/mm	40	η/(Pa · s)	0.02

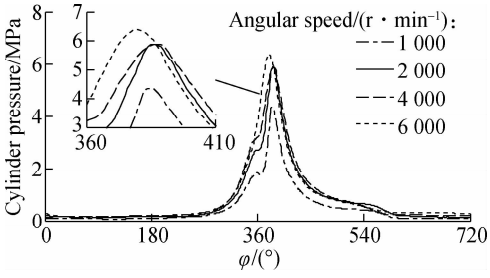

(a)

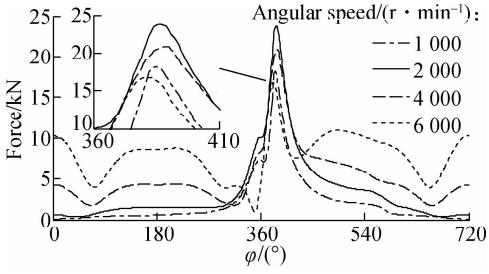

(b)

Fig. 5 Impact forces on the CB under various angular speeds. (a) Experimental combustion gas pressures; (b) Impacting forces of W_0 on the CB

crankshaft rotational angle moves from 360° to 410°, corresponding to the combustion stroke of the engine, the maximum and minimum values of W_0 are 2 000 and 6 000 r/min, respectively. However, outside the rotational angles of 360°- 410°, the maximum W_0 is 6 000 r/min. This finding may be attributed to the effect of the F_{ic} of the large-rod-end of the connecting rod and ω in Eq. (8). Thus, the LE-FPL of the CB is affected by the operating parameters of the CB. The effect of ω, r_b, and B of the CB are investigated in the next subsections.

3.1 Effect of engine speed

The relative speed between the shaft and bearing surfaces is $u_0 = \omega r_b$; thus, ω of 1 000, 2 000, 4 000, and 6 000 r/min with the corresponding W_0 are applied to study their effects on the LE-FPL of the CB, as shown in Fig. 5(b).

The simulation results of the oil film pressure and shear stress distributions on the CB surfaces under different W_0 at 2 000 r/min are shown in Fig. 6. The p values are mainly distributed over the range of 90°-180° with B, and the maximum p at 158° is 88.8 MPa. This finding is identical to the results presented in Refs. [1, 14 − 15]. The shear stress is also uniformly distributed along B.

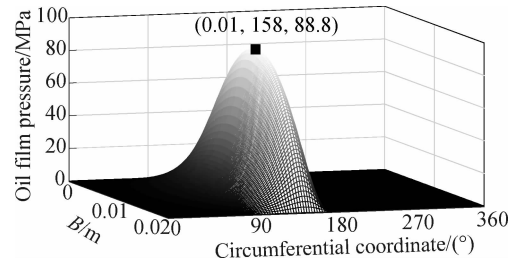

(a)

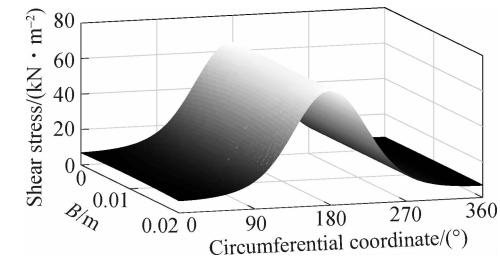

(b)

Fig. 6 Oil film pressure and shear stress on the CB surface at an angular speed of 2 000 r/min. (a) Pressure distribution; (b) Shear stress distribution

However, in the circumferential direction, the shear stress remarkably varies and peaks at 178°.

The oil film pressure and shear stress distributions at a bearing width of $B/2$ with various ω are illustrated in Fig. 7. Fig. 7(a) shows that the oil film pressure strongly depends on W_0 and ω. The maximum and minimum pressures corresponding to W_0 are also obtained at 2 000 and 6 000 r/min, and the results are shown in Fig. 5(b). The oil film shear stress mainly depends on ω, and the shear stress increases with increasing ω and vice versa.

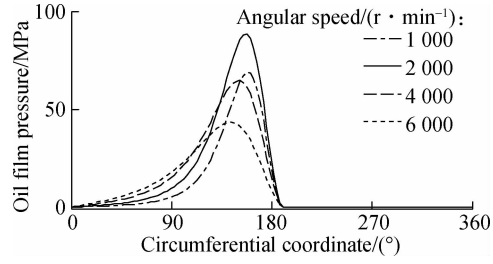

(a)

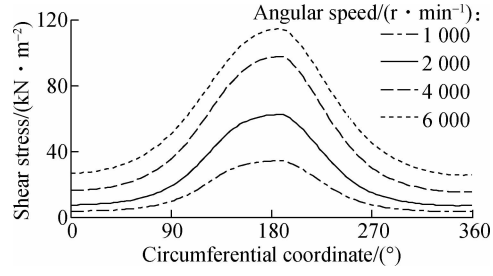

(b)

Fig. 7 Oil film pressure and shear stress at a bearing width of $B/2$ under different angular speeds. (a) Pressure distribution; (b) Shear stress distribution

The CB's load bearing capacity W and F are calculated from the results in Fig. 7 and plotted in Figs. 8(a) and (b). The W shown in Fig. 8(a) is similar to the W_0 in Fig. 5(b) under different ω because the oil film pressure varies to satisfy the condition that W is equivalent to W_0. Fig. 8 (b) reveals that F increases sharply with increasing ω. Moreover, F peaks at a high ω of 6 000 r/min, which means that the F acting on the CB is greatest at this point. This result may be due to the increase in relative velocity between the shaft and the bearing surface, which increases the shear stress and friction resistance of the oil film.

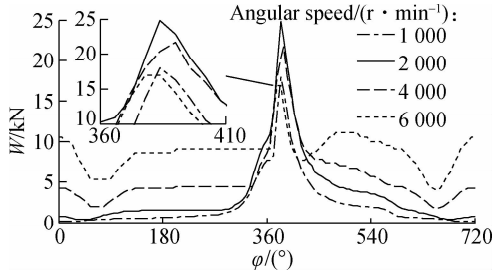

(a)

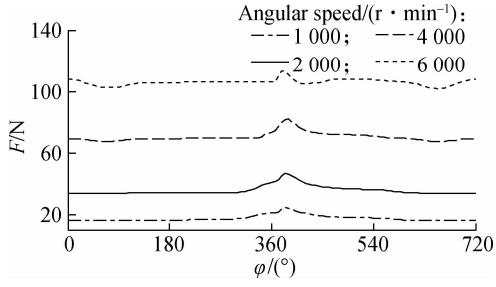

(b)

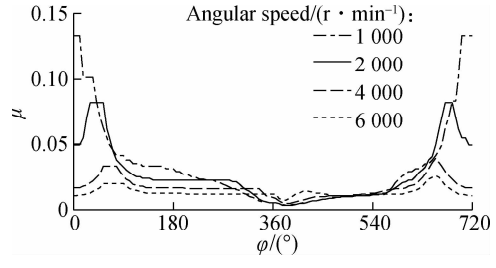

(c)

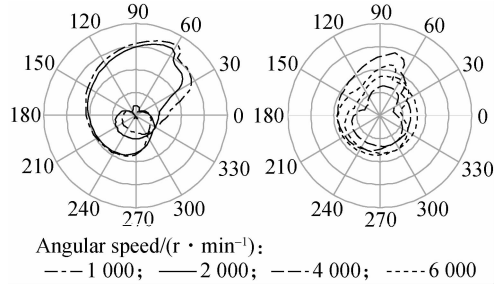

(d)

Fig. 8 Effect of angular speed on the LE-FPL. (a) CB's load bearing capacity; (b) Friction force; (c) Friction coefficient; (d) Eccentricity ratio between the journal and bearing

Fig. 8(c) presents the μ of the CB. The values of μ change with the variation of W and F and decrease with increasing ω. Comprehensive comparative analysis shows that, in the combustion stroke of the engine (i. e., a crankpin angle of 360°-410°), the maximum W_0 affects not only the CB's LE but also its engine power. In particular, when ω is maintained at 2 000 r/min, W_0 peaks, but F and μ remain relatively small. Thus, this is also a reason that most engines should work at this speed[1, 6].

The effect of ε between the journal and bearing is also investigated to analyze the stability of the CB under various ω, as shown in Fig. 8(d). The results indicate that increasing ω can reduce ε and vice versa. Moreover, ε peaks at a low ω of 1 000 r/min, and its minimum value occurs at a high ω of 6 000 r/min. Therefore, ε could also affect the LE and stability of the CB. ε shows less variation when ω is 6 000 r/min than at other speeds, which means that the lubrication capacity and the rotation of the journal are fairly stable at this point.

3.2 Effect of bearing radius

Considering the analysis above, the maximum W_0 at ω of 2 000 r/min is selected to investigate the effect of r_b and B on the LE-FPL of the engine.

The simulation results of oil film pressure and shear stress distributions at a bearing width of $B/2$ and $r_b = 15$, 20, 25, 30, 35 mm are plotted in Figs. 9(a) and (b). The results show that the oil film pressure decreases, whereas the shear stress increases as r_b gradually increases from 15 to 35 mm.

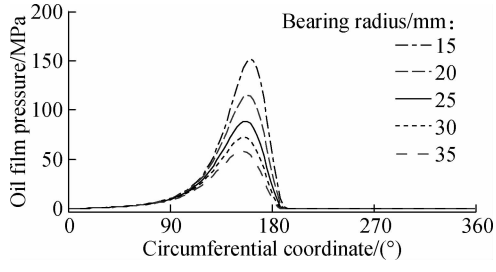

(a)

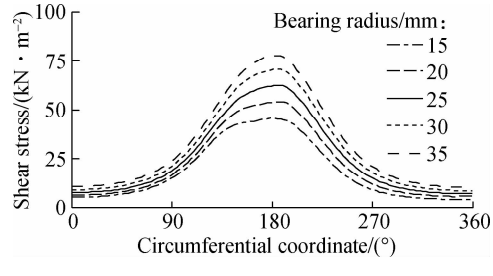

(b)

Fig. 9 Oil film pressure and shear stress at a bearing width of $B/2$ with different bearing radii. (a) Pressure distribution; (b) Shear stress distribution

Figs. 10(a) and (b), respectively, reflect changes in W and F under different r_b. Changes in r_b appear to have

less effect on W in comparison with that on W_0 under the condition of equivalent W and W_0, as illustrated in Fig. 10(a). This result may be attributed to an increase in Γ due to the increase in r_b, which leads to a decrease in oil film pressure, as shown in Fig. 9(a), to stabilize W and vice versa. This finding also verifies the accuracy and robustness of the mathematical model and algorithm developed in this study.

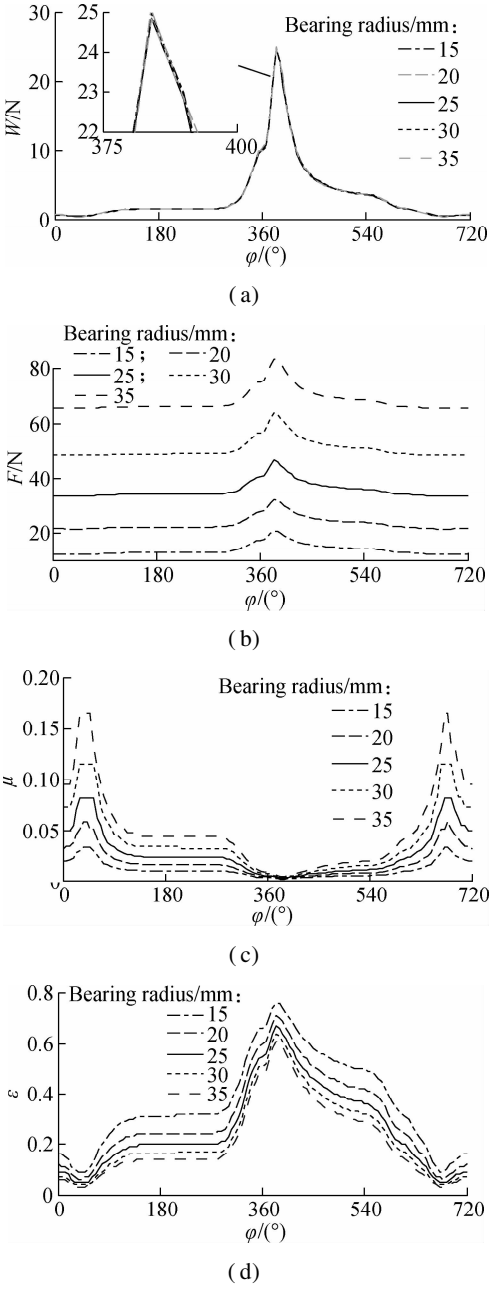

Fig. 10 Effect of bearing radius on the LE-FPL. (a) CB's load bearing capacity; (b) Friction force; (c) Friction coefficient; (d) Eccentricity ratio between the journal and bearing

Fig. 10(b) reveals that F tends to increase with increasing r_b. This finding may be attributed to increases in the relative speed of the oil film ($u_0 = \omega r_b$) and Γ affecting the oil film shear stress and friction resistance. Because W does not vary with different r_b, μ increases because of the increase in F of the CB, as shown in Fig. 10(c). Moreover, as seen in Fig. 10(d), the influence of r_b on ε is not significant, and the gap between the shaft and bearing of the CB shows an obvious tendency to decrease with increasing r_b.

3.3 Effect of bearing width

Fig. 11 demonstrates the influence of B = 10, 15, 20, 25, 30 mm on the LE-FPL under a constant W_0 at 2 000 r/min. Fig. 11(a) shows that the W generated from the oil film pressure does not change significantly in comparison with W_0 as B is gradually increased from 10 to 30 mm, likely because the oil film pressure changes to stabilize W. F and μ also tend to increase, as shown in Figs.

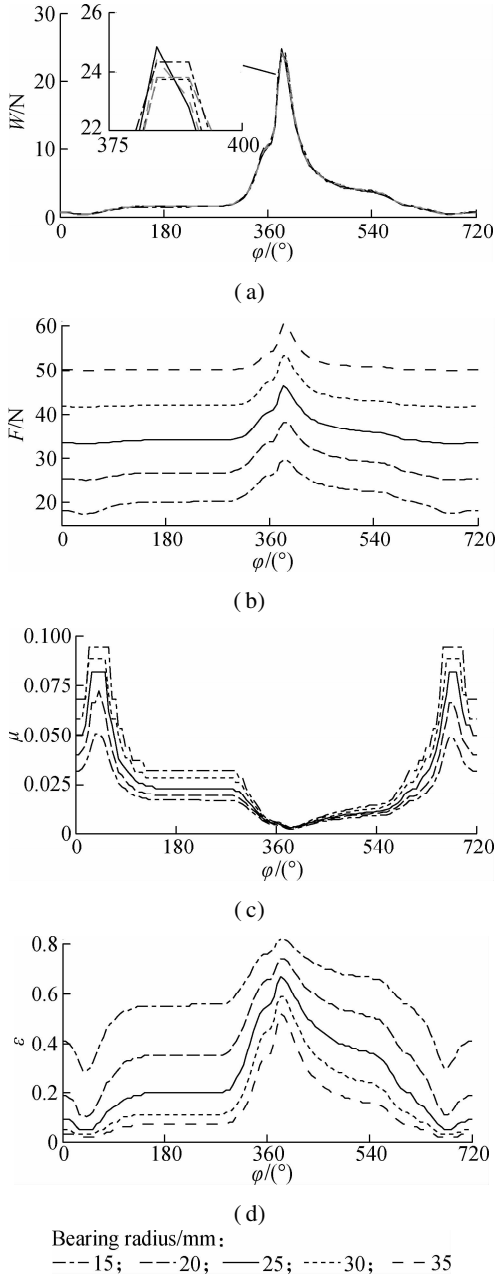

Fig. 11 Effect of bearing width on the LE-FPL. (a) CB load bearing capacity; (b) Friction force; (c) Friction coefficient; (d) Eccentricity ratio between the journal and bearing

11(b) and (c), which directly causes greater FPL. However, B variations have little effect on the ε between the journal and bearing [6, 16-17], as indicated in Fig. 11(d).

4 Conclusions

1) Increasing ω not only effectively reduces the ε between the journal and bearing but also increases the minimum h, thereby directly improving the CB LE. However, increases in ω also increase F, thereby increasing the FPL of the engine. The simulation results show that the engine's LE-FPL can be improved better when ω is maintained at 2 000 r/min.

2) Increasing the r_b or B of the CB can help decrease ε, thereby improving the LE. In addition, the dimensional change of the CB has a great influence on F and μ, which, in turn, increase the FPL of the engine.

3) Improving LE while reducing FPL is a challenging issue. Therefore, the present study not only contributes to the existing body of knowledge on the LE-FPL of automotive engines but also provides an important reference for optimal SCM design parameters to improve this engine property further.

References

[1] Zhao B, Dai X D, Zhang Z N, et al. A new numerical method for piston dynamics and lubrication analysis[J]. *Tribology International*, 2016, **94**: 395 - 408. DOI: 10.1016/j.triboint.2015.09.037.

[2] Meng X H, Ning L P, Xie Y B, et al. Effects of the connecting-rod-related design parameters on the piston dynamics and the skirt-liner lubrication[J]. *Proceedings of the Institution of Mechanical Engineers, Part D: Journal of Automobile Engineering*, 2013, **227**(6): 885 - 898. DOI: 10.1177/0954407012464025.

[3] Li Y Y, Chen G P, Sun D Y, et al. Dynamic analysis and optimization design of a planar slider-crank mechanism with flexible components and two clearance joints [J]. *Mechanism and Machine Theory*, 2016, **99**: 37 - 57. DOI: 10.1016/j.mechmachtheory.2015.11.018.

[4] Cho S H, Ahn S T, Kim Y H. A simple model to estimate the impact force induced by piston slap[J]. *Journal of Sound and Vibration*, 2002, **255**(2): 229 - 242. DOI: 10.1006/jsvi.2001.4152.

[5] Liu K, Xie Y B, Gui C L. A comprehensive study of the friction and dynamic motion of the piston assembly[J]. *Proceedings of the Institution of Mechanical Engineers, Part J: Journal of Engineering Tribology*, 1998, **212**(3): 221 - 226. DOI: 10.1243/1350650981542038.

[6] Mansouri S H, Wong V W. Effects of piston design parameters on piston secondary motion and skirt-liner friction [J]. *Proceedings of the Institution of Mechanical Engineers, Part J: Journal of Engineering Tribology*, 2005, **219**(6): 435 - 449. DOI: 10.1243/135065005x34026.

[7] Patir N, Cheng H S. Application of average flow model to lubrication between rough sliding surfaces[J]. *Journal of Lubrication Technology*, 1979, **101**(2): 220 - 229. DOI: 10.1115/1.3453329.

[8] Daniel G B, Cavalca K L. Analysis of the dynamics of a slider-crank mechanism with hydrodynamic lubrication in the connecting rod-slider joint clearance[J]. *Mechanism and Machine Theory*, 2011, **46**(10): 1434 - 1452. DOI: 10.1016/j.mechmachtheory.2011.05.007.

[9] Wang X L, Zhang J Y, Dong H. Analysis of bearing lubrication under dynamic loading consideringmicropolar and cavitating effects[J]. *Tribology International*, 2011, **44**(9): 1071 - 1075. DOI: 10.1016/j.triboint.2011.05.002.

[10] Raj A, Sinha P. Transverse roughness in short journal bearing under dynamic loading[J]. *Tribology International*, 1983, **16**(5): 245 - 251. DOI: 10.1016/0301 - 679X(83)90081 - 6.

[11] Zhang H, Hua M, Dong G N, et al. Boundary slip surface design for high speed water lubricated journal bearings[J]. *Tribology International*, 2014, **79**: 32 - 41. DOI: 10.1016/j.triboint.2014.05.022.

[12] Patir N, Cheng H S. An average flow model for determining effects of three-dimensional roughness on partial hydrodynamic lubrication[J]. *Journal of Lubrication Technology*, 1978, **100**(1): 12 - 17. DOI: 10.1115/1.3453103.

[13] Greenwood J A, Tripp J H. The contact of two nominally flat rough surfaces[J]. *Proceedings of the Institution of Mechanical Engineers*, 1970, **185**(1): 625 - 633. DOI: 10.1243/pime_proc_1970_185_069_02.

[14] Zhao B, Zhang Z N, Fang C C, et al. Modeling and analysis of planar multibody system with mixed lubricated revolute joint[J]. *Tribology International*, 2016, **98**: 229 - 241. DOI: 10.1016/j.triboint.2016.02.024.

[15] Nguyen V, Wu Z P, Le V. Optimization of crankpin bearing lubrication under dynamic loading considering effect of micro asperity contact[J]. *Industrial Lubrication and Tribology*, 2020, **72**(10): 1173 - 1179. DOI: 10.1108/ilt-02-2020-0072.

[16] Wu Z P, Nguyen V, Zhang Z H, et al. Study on curved surface design of sliding pair based on stepped topography model[J]. *Industrial Lubrication and Tribology*, 2019, **72**(1): 86 - 92. DOI: 10.1108/ilt-04-2019-0121.

[17] Wang P L, Nguyen V, Wu X Y, et al. Research on different structures of dimpled textures on improving the LE-FPL of engine[J]. *Industrial Lubrication and Tribology*, 2021. DOI: 10.1108/ilt-07-2020-0286.

[18] Christiansen C K, Walther J H, Klit P, et al. Investigation of journal orbit and flow pattern in a dynamically loaded journal bearing[J]. *Tribology International*, 2017, **114**: 450 - 457. DOI: 10.1016/j.triboint.2017.04.013.

[19] Braun M J, Hannon W M. Cavitation formation and modelling for fluid film bearings: A review[J]. *Proceedings of the Institution of Mechanical Engineers, Part J: Journal of Engineering Tribology*, 2010, **224**(9): 839 - 863. DOI: 10.1243/13506501jet772.

曲轴销轴承转速和尺寸对提高发动机功率的影响

阮文廉[1,2,3] 张建润[1] 焦仁强[2] 黄大成[1]

([1]东南大学机械工程学院，南京 211189)
([2]湖北理工学院机电工程学院，黄石 435003)
([3]Faculty of Automotive and Power Machinery Engineering, Thai Nguyen University of Technology, Thai Nguyen 23000, Vietnam)

摘要:提出了一种结合滑块曲柄机构动力学模型（SCM）和曲柄销轴承润滑模型（CB）的新方法，以全面分析 CB 的尺寸和发动机转速对润滑效率和摩擦功率损失的影响. 基于组合模型，利用在 MATLAB 中开发的算法程序求解动态方程和润滑方程. 为了提高研究结果的可靠性，采用燃烧气体压力实验数据进行仿真. 选择 CB 的承载能力(或油膜压力)、摩擦力、摩擦系数和偏心率作为评估 LE-FPL 的目标函数,分别评估发动机转速、轴承宽度和半径对 LE-FPL 的影响. 研究结果表明，减小角速度、轴承宽度或半径可以减少摩擦功率损失，但会降低发动机的润滑效率，反之亦然. 特别地，通过略微减小轴承宽度和半径或将发动机转速保持在 2 000 r/min，可以有效地改善润滑效率和摩擦功率损失.

关键词:曲柄滑块机构；曲柄销轴承;润滑性能；摩擦损失
中图分类号:U461.3